Hindawi
Journal of Nanomaterials
Volume 2019, Article ID 9367573, 8 pages
https://doi.org/10.1155/2019/9367573

Research Article

Decreased Surface Photovoltage of ZnO Photoanode Films via Optimal Annealing Temperature for Enhanced Photoelectrochemical Performance

Yichong Liu,[1] Bohuai Xiao,[1] Haijian Chen,[1] Yunchuan Li,[1] and Shuai Chang[1,2]

[1]*The State Key Laboratory of Refractories and Metallurgy, Wuhan University of Science and Technology, Wuhan 430081, China*
[2]*Institute of Advanced Materials and Nanotechnology, Wuhan University of Science and Technology, Wuhan 430081, China*

Correspondence should be addressed to Yunchuan Li; 844290658@qq.com and Shuai Chang; schang23@wust.edu.cn

Received 9 May 2018; Revised 9 August 2018; Accepted 2 October 2018; Published 27 January 2019

Guest Editor: Mohammed H. Abdul Jabbar

The electronic structure of semiconducting materials at the electrode/electrolyte interface plays a vital role in the process of photoelectrochemical (PEC) water splitting. In this work, we could reliably tune the surface defect density of ZnO films through changing the annealing temperature, thereby optimizing the PEC performance. The surface photovoltage (SPV) of ZnO films could be obtained by Kelvin probe force microscopy and compared to insightfully understand the effect of the annealing temperature on the performance of the electrode in PEC water splitting. The minimum SPV annealed at 450°C indicated low surface defect density, eventually resulting in an enhanced photoelectrochemical performance. The applied bias photo-to-current efficiency of ZnO films annealed at 450°C reached 0.237%, about 7.4 times that of unannealed ZnO photoanode. This work provides an effective method for the rational fabrication of efficient photoelectrodes for the realization of high-performance photoelectrochemical water splitting.

1. Introduction

Hydrogen generated from photoelectrochemical (PEC) water splitting has shown significant potential for solar energy conversion to meet the steady increase of energy demands [1]. In principle, the efficiency of PEC water splitting mainly depends on the following factors: (1) light absorption, (2) photogenerated charge separation and transport, and (3) surface chemical reaction [2, 3]. For a PEC system, the light absorption is determined by the bandgap of photoelectrodes, and the driving force of charge separation originates from the electric field in the depletion region at the photoelectrode/electrolyte interface. Thus, the interfacial electronic structure of semiconducting materials plays a vital role in the process of photoelectrochemical water splitting [4]. Therefore, the understanding of the change in electronic structure of semiconductor materials is favourable for the rational design of efficient photoanode. Thus, the key in a PEC system is the selection of high-performance photoelectrodes.

Although narrow-bandgap semiconductors, such as silicon and III–IV group of composites, show high light harvesting efficiency, the surface corrosion hinders their lifetime even in a sacrificial electrolyte [5, 6]. Among various N-type metal oxides [7–12], zinc oxide (ZnO) has been extensively investigated as photoanode for photoelectrochemical water splitting ascribed to its low cost, excellent electron mobility ($115–155\,cm^2 \cdot V^{-1} \cdot s^{-1}$), and appropriate conduction/valence band edges for water splitting [13–17]. As a postprocessing method, annealing has been proved to be a valid method to change the interfacial electronic structure, resulting in a significant impact on the properties of ZnO nanomaterials [18, 19]. Wu et al. [20] demonstrated that the work function of ZnO nanorod arrays exhibited a gradual increase after a decrease with the increase in the annealing temperature. Wang et al. [21] found that the improved PEC performance of ZnO nanowires (NWs) was mainly attributed to the larger depleted width in ZnO NWs caused by annealing. Further, the carrier concentration of ZnO films by electron beam

annealing is about 2~3 orders of magnitude higher than that of unannealed ZnO thin films [22]. However, there is still a lack of in-depth understanding about the change in interfacial electronic structure for the enhanced PEC performance caused by different annealing temperatures.

Previously, we have constructed various photoanodes based on ZnO nanomaterials. And surface modification materials, doping, and structure optimization were sequentially taken into combination to form ZnO-based composite nanostructures, in which each component worked synergistically to compensate each other [13–16]. In conclusion, there are some significant differences between previous works and current work as for the following aspects. Previous works put emphasis on the realization of highly efficient photoanode based on ZnO nanomaterials to raise the light harvesting efficiency, reduce the charge recombination, and accelerate the surface reaction. However, multistep and complex processes are always introduced into these strategies. Thus, this work adopts a one-step process and posttreatment to tune the PEC performance, and we mainly focused on the change of interfacial electronic structure by the KPFM. The surface photovoltage (SPV) of ZnO films under different annealing temperatures was obtained through calculating the difference between the surface potentials under UV illumination and in the dark measured by KPFM. After annealing at 450°C, the minimum SPV of ZnO films indicated low defect density, which contributed to the improved photocurrent density and enhanced photoelectrochemical performance. This simple and novel method also allows us to have more fundamental understanding of the effects of ZnO itself on the PEC performance.

2. Materials and Methods

Commercially available indium tin oxide- (ITO-) coated glass ($2 \times 2\,\text{cm}^2$) was used as the substrate. ITO substrates were sequentially sonicated in acetone, isopropanol, ethanol, and deionized water, each for 10 minutes, and then dried with nitrogen gas flow. The ZnO film was deposited on the ITO substrate via the radiofrequency (RF) magnetron sputtering method as reported [23]. After deposition, ZnO films were annealed in a vacuum drying oven at 350°C, 450°C, and 550°C for 2 hours, respectively. The corresponding samples were named ZnO-350, ZnO-450, and ZnO-550.

The morphology and crystalline structure of the ZnO film were characterized by field-emission scanning electron microscopy (FESEM, FEI QUANTA 3D) and X-ray diffraction (XRD) (Rigaku DMAX-RB with Cu Kα radiation), respectively. The light absorption and photoluminescence spectrum were recorded by a UV-vis spectrophotometer (UV-2500, Shimadzu, Japan) and a continuous He-Cd (325 nm) laser as an excitation source, respectively. KPFM measurements were tested under a commercially available atomic force microscope (ICON, Bruker Inc.) in lift mode at about 25°C. PtIr-coated silicon cantilevers (Olympus, OSCM-PIT) with a nominal resonance frequency of 75 kHz were used as conductive probes.

A copper wire was secured on the exposed conductive parts of ITO with a silver conducting paint, and the rest of the substrate was subsequently encapsulated with epoxy resin except the active working area, confirming the successful preparation of the photoanode. A three-electrode system used for various electrochemical measurements on an electrochemical workstation (Solartron SI 1287/SI 1260) consists of a photoanode as the working electrode, a coiled Pt wire as the counter electrode, and an Ag/AgCl reference electrode. Neutral aqueous Na_2SO_4 solution (0.5 M) was chosen as the electrolyte. The simulated sunlight provided by a solar simulator (Oriel, 91159A) is incident from the front of the photoanode, and the intensity of the simulated sunlight was $60\,\text{mW/cm}^2$ measured by a Si diode (Newport). The applied bias photo-to-current efficiency (η_{ABPE}) was calculated from $J_{\text{ph}} - V$ curves, assuming 100% faradaic efficiency through the following equation [24]:

$$\eta_{\text{ABPE}} = \frac{I\left(1.23 - V_{\text{app}}\right)}{P_{\text{light}}}, \tag{1}$$

where V_{app} is the applied external potential versus the reversible hydrogen electrode (RHE). I is the externally measured current density at V_{app}. P_{light} is the power density of the incident light. The potentials were measured versus the Ag/AgCl reference electrode and converted to the RHE scale using the Nernst function:

$$E_{\text{RHE}} = E_{\text{Ag/AgCl}} + E^{\circ}_{\text{Ag/AgCl}} + 0.059\text{pH}, \tag{2}$$

where E_{RHE} is the converted potential versus RHE. $E_{\text{Ag/AgCl}}$ is the external potential measured against the Ag/AgCl reference electrode. $E^{\circ}_{\text{Ag/AgCl}}$ is the standard electrode potential of the Ag/AgCl reference electrode (0.1976 V versus RHE at 25°C).

3. Results and Discussion

Figure 1(a) exhibits a representative cross-sectional scanning electron microscope (SEM) image of the ZnO film on the ITO prior to annealing, indicating that the film is composed of multiple ZnO columnar grains. The grain size calculated from the top view image in the inset of Figure 1(a) is in the range of 30–100 nm. Furthermore, the corresponding XRD pattern is used to characterize the structure of an unannealed ZnO film. As shown in Figure 1(b), XRD of ZnO films exhibits that all diffraction peaks can be corresponded to the planes of highly crystalline ZnO (JCPDS file no. 36-1451). And the apparent diffraction peak of (002) at 34.4° demonstrates that the ZnO film is grown preferentially along c-axis direction on the ITO [25].

The schematic illustration of the ZnO film on the ITO upon the bandgap illumination is shown in Figure 2(a). Under simulated sunlight, electrons and holes are generated in the conduction band (E_{CB}) and valence band (E_{VB}), respectively. The photogenerated electrons transfer to the Pt electrode for the hydrogen evolution in the PEC cell device. On the other hand, the photogenerated holes in E_{VB}

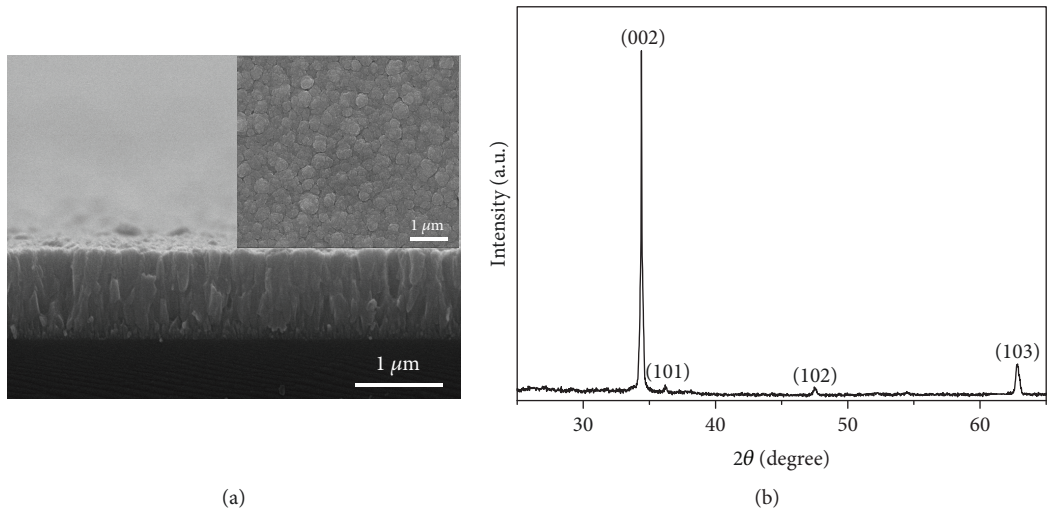

Figure 1: (a) Cross-sectional SEM image of the RF-sputtered ZnO film on the ITO prior to annealing. The inset is the top view image. (b) The corresponding XRD pattern of the deposited film.

of ZnO participate in the oxidation evolution to finish the whole process.

In order to study the photoelectrochemical properties of the prepared photoanodes, the PEC measurements of various as-prepared photoanodes were characterized by linear sweep voltammetry (LSV) curves in the dark and under simulated sunlight illumination. A very small dark photocurrent in the scale of 10^{-3} mA/cm^2 is shown in Figure 2(b), implying that the observed photocurrent is related to the photogenerated charge carriers. Under illumination, a significant increase in photocurrent density was observed, and the ZnO-450 photoanode exhibited the highest photocurrent density in the whole investigated potential range, ascribed to the lowest density of trap states at the surface among those of other samples. The photocurrent density of unannealed ZnO, ZnO-350, ZnO-450, and ZnO-550 reached 0.19, 0.559, 0.586, and 0.457 mA/cm^2 at 1 V vs. Ag/AgCl, respectively. According to (1) and (2), the ABPE of different photoanodes was calculated from the LSV curve. As shown in Figure 3(c), the ZnO-450 photoanode exhibited the highest efficiency of 0.237%, about 7.4 times that of the unannealed ZnO photoanode (0.032%).

To attain a deep understanding of the PEC performance, electrochemical impedance spectroscopy (EIS) was used to explore the electrochemical behavior at the photoelectrode/electrolyte interface at 0 V vs. Ag/AgCl under white light illumination. Figure 2(d) reveals the typical EIS Nyquist plots for four different photoanodes, and the equivalent circuit in Figure 2(d) was used to fit the Nyquist plots, in which R_s, R_{ct}, and CPE represented series resistance, interfacial charge-transfer resistance at the photoelectrode/electrolyte interface, and constant phase angle element, respectively. The smaller size of the arc in an EIS Nyquist plot indicated a faster charge transfer and less recombination at the photoelectrode/electrolyte interface. The results obtained by fitting revealed that the corresponding R_{ct} of unannealed ZnO, ZnO-350, ZnO-450, and ZnO-550 was 5.18, 2.6, 2.18, and 3.98 kΩ, respectively. The smallest R_{ct} of the ZnO-450 photoanode could result in the highest photocurrent density and ABPE consistent with the LSV and ABPE curve shown in Figures 2(b) and 2(c).

To explore the photocurrent improvement, light absorption properties of ZnO films annealed under different temperatures were investigated by the UV-vis absorbance spectra. As shown in Figure 4(a), all the samples showed similar optical absorption in the UV region. As the annealing temperature increases, the optical absorption edges showed a slight red shift. Further, the optical bandgap of different samples was estimated based on the following equation [26]:

$$(\alpha h\nu)^n = A\left(h\nu - E_g\right), \tag{3}$$

where α is the absorption coefficient of the material, $h\nu$ is the energy of photon, n represents the index which depends on the electronic transition of the semiconductor (for direct bandgap semiconductor ZnO, $n = 2$), and A is the proportionality constant related to the material. Therefore, the bandgap energy could be obtained from the intercept of the tangent line in the plot of $(\alpha h\nu)^2$ versus energy. As shown in Figure 4(b), the optical bandgap decreased from 3.11 eV to 3.09 eV as the annealing temperature increased. Thus, the negligible deviation (~0.02 eV) meant that the light absorption is not the dominating reason for the improvement of the photocurrent.

To reveal the effect of annealing temperature on the charge separation, the room temperature photoluminescence (PL) spectra were investigated to study the change of the surface defect density of ZnO films annealed at different temperatures. As shown in Figure 4(c), the samples showed two main peaks: the sharp one around 390 nm was ascribed to the near-band-edge (NBE) emission and the other broad one was in the range of 440–660 nm corresponding to the intrinsic defect-related energy [27, 28]. In Figure 4(d), a red

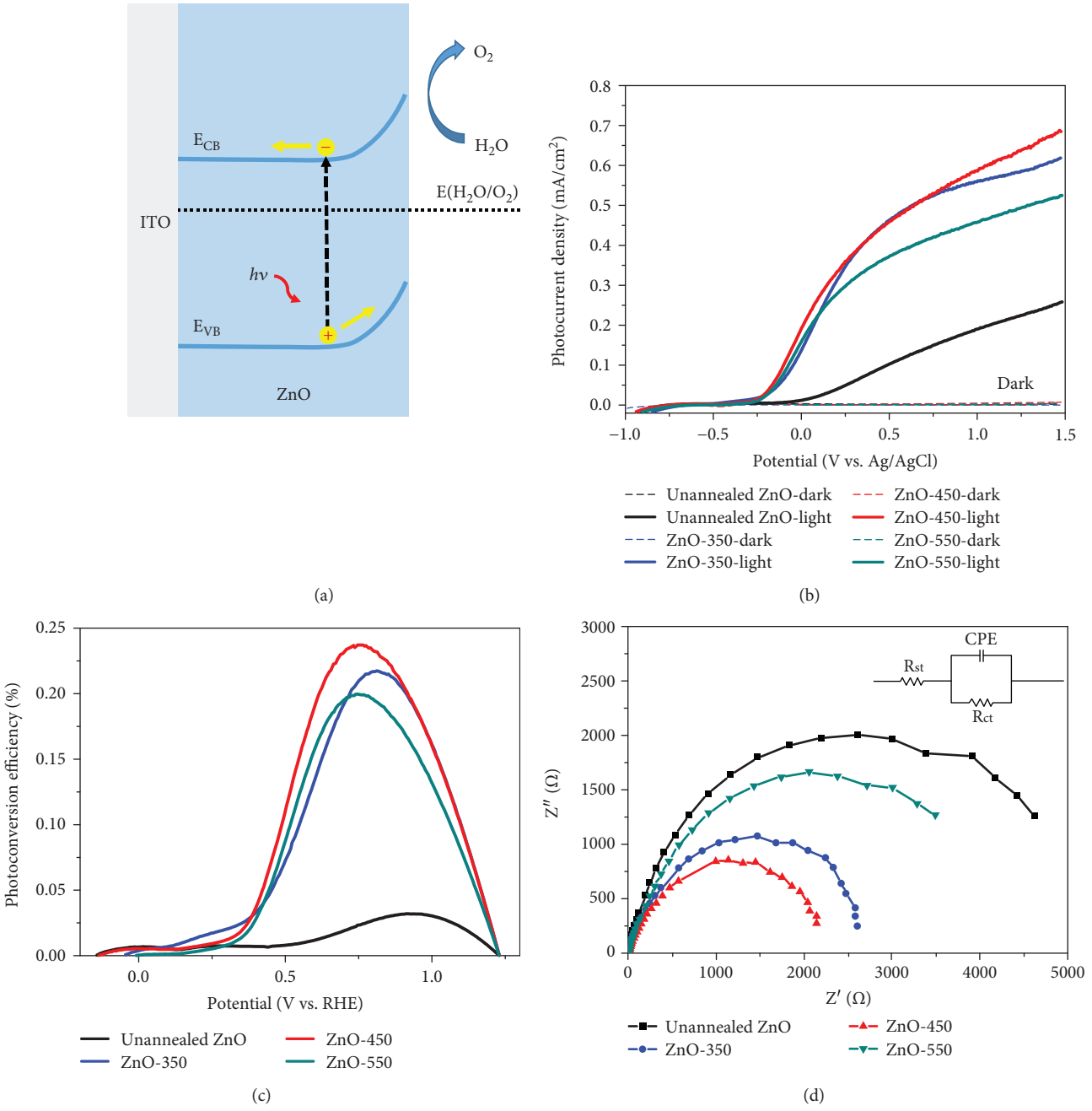

Figure 2: (a) Cross-sectional schematic and energy band alignment of the ZnO photoanode for water splitting. Comparisons of PEC properties of four different photoanodes: unannealed ZnO (black), ZnO-350 (blue), ZnO-450 (red), and ZnO-550 (cyan). (b) Linear sweep voltammetry measurements in the dark and under illumination, (c) the corresponding applied bias photo-to-current efficiency as a function of applied potential vs. RHE, and (d) Nyquist plots measured at an applied potential of 0 V vs. Ag/AgCl under illumination. The inset is the equivalent circuit used to fit the Nyquist plots.

shift of NBE emission peak was observed with the increase in annealing temperature, which is consistent with the change of optical bandgap in Figure 4(b). When the annealing temperature was no more than 450°C, the intensity of broad deep-level (DL) emission decreased ascribed to the improved crystalline quality after annealing. However, when the annealing temperature reached 550°C, the intensity of DL emission revealed a significant increase due to the increased probability of the radiative recombination which is associated with the deep-level emission. Therefore, the low intensity of DL emission of ZnO-450 indicated reduced electron-hole recombination.

To further characterize the surface defect density of ZnO films annealed at different temperatures, Kelvin probe force microscopy (KPFM) was employed under dark and light conditions to measure the surface potential difference [29–31]. As shown in Figure S1 in Supplementary Materials, the contact potential difference (V_{CPD}) between a sample and

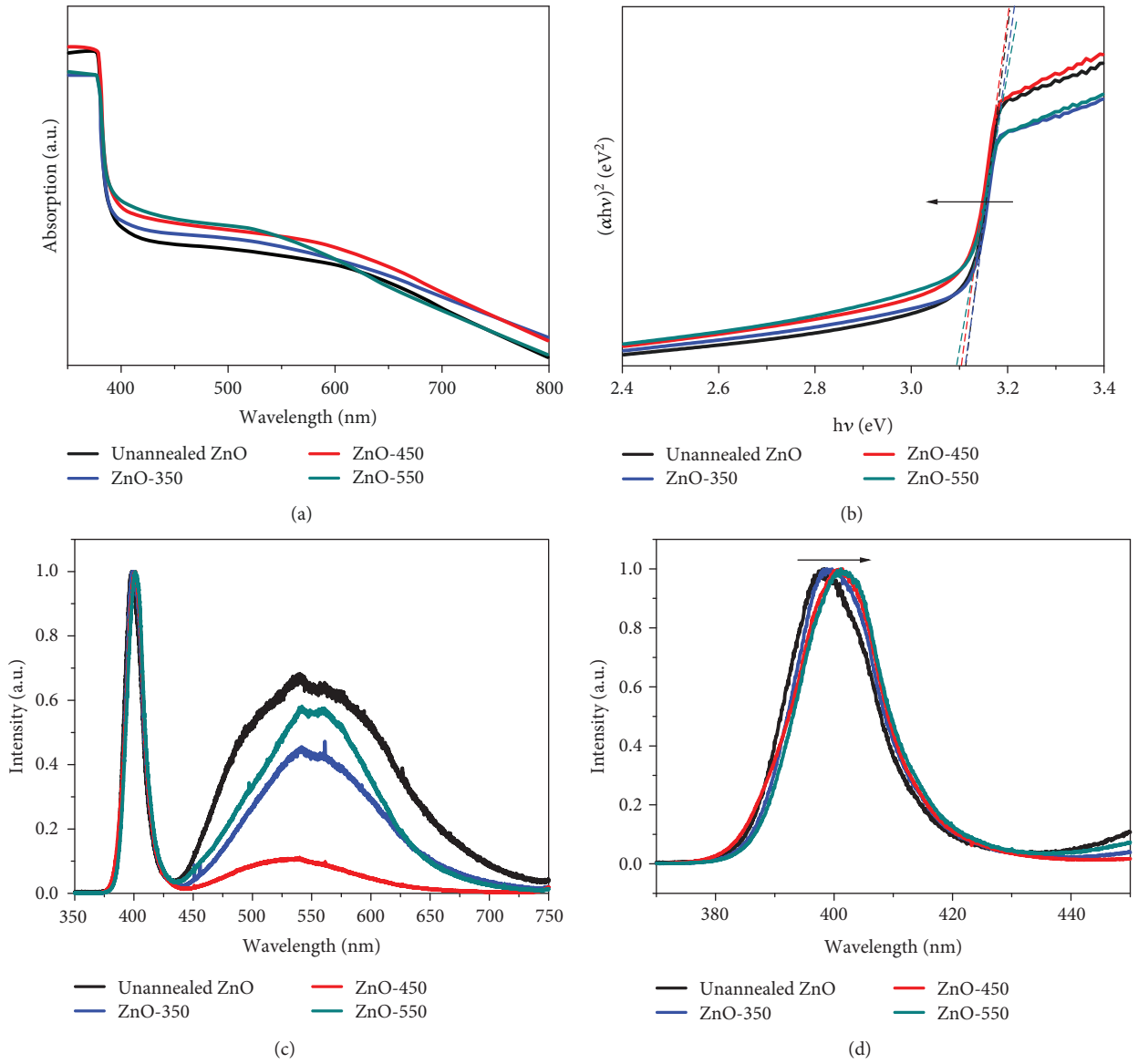

Figure 3: (a) UV-vis absorption spectra and (b) the corresponding $(\alpha h\nu)^2$ vs. $h\nu$ curves of unannealed ZnO, ZnO-350, ZnO-450, and ZnO-550. Photoluminescence (PL) spectra of unannealed ZnO, ZnO-350, ZnO-450, and ZnO-550: (c) 300~720 nm and (d) 370~450 nm.

a tip was acquired for different samples in the dark and under UV illumination, respectively, and the corresponding average V_{CPD} was statistically analysed as shown in Figures 3(a)–3(d). As shown in Figure 4(f), the difference in work function in the dark and under UV illumination is defined as the surface photovoltage (SPV), which could be acquired based on the following equations [4, 32, 33]:

$$V_{CPD} = \frac{\varphi_{tip} - \varphi_{sample}}{q}, \tag{4}$$

$$\begin{aligned} SPV &= \varphi_{sample\text{-}dark} - \varphi_{sample\text{-}light} \\ &= q\left(V_{CPD\text{-}light} - V_{CPD\text{-}dark}\right), \end{aligned} \tag{5}$$

where φ_{tip} and φ_{sample} are the work functions of the tip and sample, respectively, and q is the electronic charge. Figure 4(e) exhibits the average V_{CPD} and SPV of different samples, and the SPV of unannealed ZnO, ZnO-350, ZnO-450, and ZnO-550 was 95.8 mV, 73.3 mV, 71.6 mV, and 89.9 mV, respectively. As the SPV was used to demonstrate the change of the band bending at the photoelectrode/electrolyte surface, the SPV could be used to indicate the density of surface states [30, 34]. Thus, the minimum SPV value of ZnO-450 suggested the low density of trap states at the surface, which was in agreement with the results of photoluminescence spectra in Figure 4(c) and contributed to the enhancement of the PEC performance.

4. Conclusions

In summary, the photoelectrochemical performances of ZnO films on the ITO substrate were investigated through the work function study at the electrode/electrolyte interface

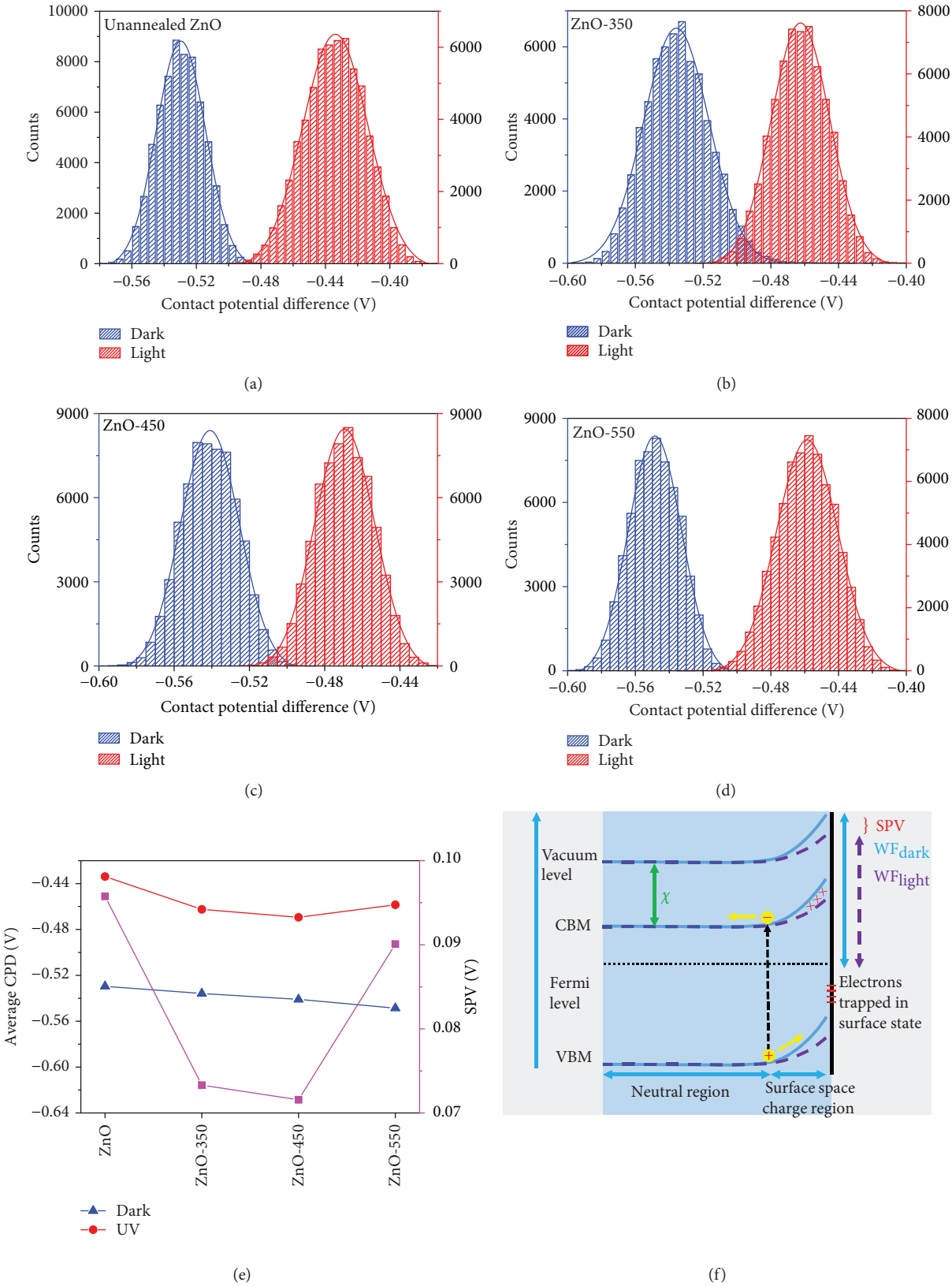

Figure 4: The statistical CPD acquired from KPFM mapping in the dark and under illumination: (a) unannealed ZnO, (b) ZnO-350, (c) ZnO-450, and (d) ZnO-550, respectively. (e) Average CPD in the dark and under illumination to the left scale and SPV of different samples to the right scale. (f) Schematic energy band diagram for the generation of surface photovoltage (SPV) at the ZnO surface (CBM: conduction band minimum; VBM: valence band maximum; χ: electron affinity). The solid lines and the dotted lines represent the condition in the dark and light, respectively.

under different annealing temperatures. After annealing at 450°C, the minimum SPV of ZnO films indicated low defect density, which contributed to the improved photocurrent density and enhanced photoelectrochemical performance. The ZnO films annealed under 450°C exhibited an efficiency of 0.237%, which was much higher than that of unannealed ZnO films (0.032%). As a whole, this work provided a potential method to design innovative photoanodes for photoelectrochemical water splitting.

Data Availability

The data used to support the findings of this study are available from the corresponding author upon request.

Conflicts of Interest

There is no conflict of interest regarding the publication of this paper.

Acknowledgments

The authors acknowledge the funding support from the Project of Thousand Youth Talents and National Natural Science Foundation of China (NNSFC) (21705122).

Supplementary Materials

The images of contact potential differences in the dark and under UV illumination measured by KPFM are provided. *(Supplementary Materials)*

References

[1] S. K. Saraswat, D. D. Rodene, and R. B. Gupta, "Recent advancements in semiconductor materials for photoelectrochemical water splitting for hydrogen production using visible light," *Renewable & Sustainable Energy Reviews*, vol. 89, pp. 228–248, 2018.

[2] Z. Chen, T. F. Jaramillo, T. G. Deutsch et al., "Accelerating materials development for photoelectrochemical hydrogen production: standards for methods, definitions, and reporting protocols," *Journal of Materials Research*, vol. 25, no. 01, pp. 3–16, 2011.

[3] S. J. A. Moniz, S. A. Shevlin, D. J. Martin, Z. X. Guo, and J. Tang, "Visible-light driven heterojunction photocatalysts for water splitting – a critical review," *Energy & Environmental Science*, vol. 8, no. 3, pp. 731–759, 2015.

[4] W.-H. Lin, J. J. Wu, M. M. C. Chou, Y. M. Chang, and M. Yoshimura, "Charge transfer in Au nanoparticle–nonpolar ZnO photocatalysts illustrated by surface-potential-derived three-dimensional band diagram," *The Journal of Physical Chemistry C*, vol. 118, no. 34, pp. 19814–19821, 2014.

[5] M. G. Walter, E. L. Warren, J. R. McKone et al., "Solar water splitting cells," *Chemical Reviews*, vol. 110, no. 11, pp. 6446–6473, 2010.

[6] A. Fujishima and K. Honda, "Electrochemical photolysis of water at a semiconductor electrode," *Nature*, vol. 238, no. 5358, pp. 37-38, 1972.

[7] I. S. Cho, Z. Chen, A. J. Forman et al., "Branched TiO2 nanorods for photoelectrochemical hydrogen production," *Nano Letters*, vol. 11, no. 11, pp. 4978–4984, 2011.

[8] G. Wang, Y. Ling, D. A. Wheeler et al., "Facile synthesis of highly photoactive α-Fe_2O_3-based films for water oxidation," *Nano Letters*, vol. 11, no. 8, pp. 3503–3509, 2011.

[9] D. A. Wheeler, G. Wang, Y. Ling, Y. Li, and J. Z. Zhang, "Nanostructured hematite: synthesis, characterization, charge carrier dynamics, and photoelectrochemical properties," *Energy & Environmental Science*, vol. 5, no. 5, article 6682, 2012.

[10] Y. J. Hwang, C. Hahn, B. Liu, and P. Yang, "Photoelectrochemical properties of TiO_2 nanowire arrays: a study of the dependence on length and atomic layer deposition coating," *ACS Nano*, vol. 6, no. 6, pp. 5060–5069, 2012.

[11] H. Han, S. Kment, F. Karlicky et al., "Sb-doped SnO_2 nanorods underlayer effect to the α-Fe_2O_3 nanorods sheathed with TiO_2 for enhanced photoelectrochemical water splitting," *Small*, vol. 14, no. 19, article 1703860, 2018.

[12] S. Wang, P. Chen, Y. Bai, J. H. Yun, G. Liu, and L. Wang, "New $BiVO_4$ dual photoanodes with enriched oxygen vacancies for efficient solar-driven water splitting," *Advanced Materials*, vol. 30, no. 20, article 1800486, 2018.

[13] Y. Liu, Y. Gu, X. Yan et al., "Design of sandwich-structured ZnO/ZnS/Au photoanode for enhanced efficiency of photoelectrochemical water splitting," *Nano Research*, vol. 8, no. 9, pp. 2891–2900, 2015.

[14] Y. Liu, X. Yan, Z. Kang et al., "Synergistic effect of surface plasmonic particles and surface passivation layer on ZnO nanorods array for improved photoelectrochemical water splitting," *Scientific Reports*, vol. 6, no. 1, article 29907, 2016.

[15] Y. Liu, Z. Kang, H. Si et al., "Cactus-like hierarchical nanorod-nanosheet mixed dimensional photoanode for efficient and stable water splitting," *Nano Energy*, vol. 35, pp. 189–198, 2017.

[16] Y. Liu, Z. Kang, S. Zhang et al., "Ferroelectric polarization-enhanced charge separation in a vanadium-doped ZnO photoelectrochemical system," *Inorganic Chemistry Frontiers*, vol. 5, no. 7, pp. 1533–1539, 2018.

[17] C. Zhang, M. Shao, F. Ning et al., "Au nanoparticles sensitized ZnO nanorod@nanoplatelet core–shell arrays for enhanced photoelectrochemical water splitting," *Nano Energy*, vol. 12, pp. 231–239, 2015.

[18] J. K. Cooper, Y. Ling, C. Longo, Y. Li, and J. Z. Zhang, "Effects of hydrogen treatment and air annealing on ultrafast charge carrier dynamics in ZnO nanowires under in situ photoelectrochemical conditions," *The Journal of Physical Chemistry C*, vol. 116, no. 33, pp. 17360–17368, 2012.

[19] M. Baek, D. Kim, and K. Yong, "Simple but effective way to enhance photoelectrochemical solar-water-splitting performance of ZnO nanorod arrays: charge-trapping $Zn(OH)_2$ annihilation and oxygen vacancy generation by vacuum annealing," *ACS Applied Materials & Interfaces*, vol. 9, no. 3, pp. 2317–2325, 2017.

[20] H. Wu, M. Xue, J. Ou, F. Wang, and W. Li, "Effect of annealing temperature on surface morphology and work function of ZnO nanorod arrays," *Journal of Alloys and Compounds*, vol. 565, pp. 85–89, 2013.

[21] L. Wang, X. Gu, Y. Zhao, and Y. Qiang, "Enhanced photoelectrochemical properties of ZnO nanowire arrays annealed in air," *Journal of Materials Science: Materials in Electronics*, vol. 29, no. 5, pp. 4058–4064, 2018.

[22] Y. Li, Y. Men, X. Kong, Z. Gao, L. Han, and X. Li, "Enhanced electrical properties of ZnO transparent conducting films prepared by electron beam annealing," *Applied Surface Science*, vol. 428, pp. 191–198, 2018.

[23] P. Lin, X. Yan, Y. Liu, P. Li, S. Lu, and Y. Zhang, "A tunable ZnO/electrolyte heterojunction for a self-powered photodetector," *Physical Chemistry Chemical Physics*, vol. 16, no. 48, pp. 26697–26700, 2014.

[24] J. W. Ager, M. R. Shaner, K. A. Walczak, I. D. Sharp, and S. Ardo, "Experimental demonstrations of spontaneous, solar-driven photoelectrochemical water splitting," *Energy & Environmental Science*, vol. 8, no. 10, pp. 2811–2824, 2015.

[25] A. U. Pawar, C. W. Kim, M. J. Kang, and Y. S. Kang, "Crystal facet engineering of ZnO photoanode for the higher water splitting efficiency with proton transferable Nafion film," *Nano Energy*, vol. 20, pp. 156–167, 2016.

[26] S. J. A. Moniz, J. Zhu, and J. Tang, "1D Co-Pi modified $BiVO_4$/ZnO junction cascade for efficient photoelectrochemical water cleavage," *Advanced Energy Materials*, vol. 4, no. 10, p. 1301590, 2014.

[27] X. Peng, J. Xu, H. Zang, B. Wang, and Z. Wang, "Structural and PL properties of Cu-doped ZnO films," *Journal of Luminescence*, vol. 128, no. 3, pp. 297–300, 2008.

[28] P. T. Hsieh, Y. C. Chen, C. M. Wang, Y. Z. Tsai, and C. C. Hu, "Structural and photoluminescence characteristics of ZnO films by room temperature sputtering and rapid thermal annealing process," *Applied Physics A*, vol. 84, no. 3, pp. 345–349, 2006.

[29] S. Lu, Q. Liao, J. Qi et al., "The enhanced performance of piezoelectric nanogenerator via suppressing screening effect with Au particles/ZnO nanoarrays Schottky junction," *Nano Research*, vol. 9, no. 2, pp. 372–379, 2016.

[30] H. Si, Q. Liao, Z. Kang et al., "Deciphering the NH_4PbI_3 intermediate phase for simultaneous improvement on nucleation and crystal growth of perovskite," *Advanced Functional Materials*, vol. 27, no. 30, article 1701804, 2017.

[31] W. Zhang, S. Pathak, N. Sakai et al., "Enhanced optoelectronic quality of perovskite thin films with hypophosphorous acid for planar heterojunction solar cells," *Nature Communications*, vol. 6, no. 1, article 10030, 2015.

[32] Y. Zhang, O. Pluchery, L. Caillard et al., "Sensing the charge state of single gold nanoparticles via work function measurements," *Nano Letters*, vol. 15, no. 1, pp. 51–55, 2015.

[33] H. Yoo, C. Bae, Y. Yang et al., "Spatial charge separation in asymmetric structure of Au nanoparticle on TiO_2 nanotube by light-induced surface potential imaging," *Nano Letters*, vol. 14, no. 8, pp. 4413–4417, 2014.

[34] S. M. Jain, Z. Qiu, L. Häggman et al., "Frustrated Lewis pair-mediated recrystallization of $CH_3NH_3PbI_3$ for improved optoelectronic quality and high voltage planar perovskite solar cells," *Energy & Environmental Science*, vol. 9, no. 12, pp. 3770–3782, 2016.